Evolution and chemical characteristics of organic aerosols during wintertime $PM_{2.5}$ episodes in Shanghai, China: Insights gained from online measurements of organic molecular markers

Shuhui Zhu[1,2], Min Zhou[1], Liping Qiao[1], Dan Dan Huang[1], Qiongqiong Wang[3], Shan Wang[2], Yaqin Gao[1],
Shengao Jing[1], Qian Wang[1], Hongli Wang[1], Changhong Chen[1], Cheng Huang[1,*], Jian Zhen Yu[2,3,*]

[1]State Environmental Protection Key Laboratory of the Cause and Prevention of Urban Air Pollution Complex, Shanghai
Academy of Environmental Sciences, Shanghai, China

[2]Division of Environment and Sustainability, Hong Kong University of Science and Technology, Hong Kong, China

[3]Department of Chemistry, Hong Kong University of Science and Technology, Hong Kong, China

Correspondence to: Jian Zhen Yu (jian.yu@ust.hk) and Cheng Huang (huangc@saes.sh.cn)

Abstract. Organic aerosol (OA) is a significant part of urban fine particulate matter ($PM_{2.5}$) and a lack of detailed knowledge of their sources has increasingly hindered the improvement of air quality in China in recent years as significant reductions have been achieved in inorganic ion constituents. In this study, a wide range of organic molecular markers in $PM_{2.5}$ were monitored with a bihourly time resolution using a Thermal desorption Aerosol Gas chromatograph system (TAG) in urban Shanghai in winter 2019. The molecular marker data have provided a unique source tracking ability in characterizing the evolution of organic aerosols during nine wintertime episodic events. Episodes primarily influenced by local air masses were characterized with higher proportions in $PM_{2.5}$ and mass increments of both primary and secondary OA. Rapid increases in both absolute mass concentration and relative proportion was observed for primary and secondary OA markers indicative of vehicle emissions (e.g., alkanes, hopanes, and 2,3-dihydroxy-4-oxopentanoic acid), as well as cooking activities (e.g., saturated and unsaturated fatty acids, and C_9 acids). In comparison, episodes under significant influences of transported air mass were typically associated with a predominant $PM_{2.5}$ contribution from secondary inorganic aerosols and enhanced OA contribution from biomass burning activities. The latter was evident from the tracer data (e.g., levoglucosan, aromatic polycarboxylic acids, and nitro-aromatic compounds). Secondary OA markers associated with later generation products of hydrocarbon oxidation process, such as C_{3-5} dicarboxylic acids, were the most deficient during local episodes while notably enhanced during the episodes under influence of transported air masses, reflecting different extent and pathways of atmospheric aging processing. The ability of distinguishing the variations of OA evolution during different types of episodes demonstrates the value of online organic molecular measurements to episodic analysis. The results indicate that control of local urban sources such as vehicular and cooking emissions would lessen severity of local episodes while regional control of precursors for secondary inorganic aerosols and biomass burning activities would reduce $PM_{2.5}$ episodes under synoptic conditions conducive for regional transport.

1. Introduction

Fine particulate matter (PM$_{2.5}$) pollution has been one of the most prominent environmental issues in recent decades due to rapid industrialization and urbanization worldwide. In China, high concentration of PM$_{2.5}$ has resulted in significant drop of visibility (Zhang et al., 2012) and adverse impacts in mortality (Chen et al., 2017; Liu et al., 2017). Annual PM$_{2.5}$ concentration in China has been decreasing gradually over the past years with the implementation of a series of emission control measures focusing on reducing pollutions from energy usage, industrial processes and road transportation (Ding et al., 2019), however, haze episodes accompanied with abrupt elevation of PM$_{2.5}$ concentration still occur frequently in the cold season (Fan et al., 2021; Guo et al., 2020; Mao et al., 2019; Sun et al., 2019). According to the Report on the State of the Ecology and Environment (2019), on daily average, nearly five out of the 337 prefectural-level cities in China were under heavy or very heavy pollution with PM$_{2.5}$ as the leading pollutant.

The accumulation of PM$_{2.5}$ is a combined result of source emissions, atmospheric dynamics, chemical transformation and wet/dry deposition. Many studies have shown that either local emissions or regional transport coupled with secondary processes under certain meteorological conditions are major contributors to short-term haze episodes in China (Cai et al., 2017; Chen & Wang, 2015; Huang et al., 2014; Li et al., 2016; Liu et al., 2017; Ren et al., 2014; Wang et al., 2015; Wang et al., 2014a; Zhao et al., 2013). For example, Liu et al. (2014) and Wang et al. (2015) investigated several cases of severe haze pollution in north China and identified that local traffic emissions together with enhanced coal combustion activities were the main causes of winter haze episodes. Besides primary emissions, significant contribution of secondary chemical transformation to haze episodes is also documented in the literature (Huang et al., 2014; Tao et al., 2017). Huang et al. (2014) reported that secondary species contributed 30~77% and 44~71% of PM2.5 and of organic aerosol, respectively, during haze episodes in China. He also found that the contribution of secondary organic aerosol (SOA) to PM$_{2.5}$ episodes was on average of similar importance as secondary inorganic aerosol (SIA), suggesting that organic aerosols (OA) played an important role in controlling China's PM$_{2.5}$ levels.

The chemical characteristics and formation mechanisms of OA during episodic events have been extensively investigated by a number of studies with the application of state-of-the-art online measurement techniques (He et al., 2020; Zeng et al., 2022; W. Zhu et al., 2021). For example, Zeng et al. (2022) adopted an aerosol mass spectrometer (AMS) to analyze OA compositions in Shanghai during different episodic events. Their results showed that aged OA from long-range transport (aged in space) had a similar degree of oxygenation compared to the prolonged local oxidation (aged in time). W. Zhu et al. (2021) also employed AMS to investigate OA evolution in urban Shanghai. They found that aqueous-phase processing played a more important role in aged SOA formation in summer and winter while during PM episodes in spring, both aqueous-phase and photochemical processing contributed significantly to fresh SOA formation. In these studies, however, important molecular information of OA compositions was missing, which impedes us to develop a deeper understanding of OA sources and formation mechanisms that connect with specific precursors or precursor groups.

In this work, a field campaign was conducted in an urban site in Shanghai to characterize the evolution of haze episodes during the winter of 2019. During this campaign, 98 organic compounds in PM$_{2.5}$ were continuously monitored using a Thermal desorption Aerosol Gas chromatograph system (TAG) with a bihourly time resolution, along with hourly measurements of PM$_{2.5}$ major components and trace elements. The continuous online measurements of primary and secondary OA tracers by TAG have enabled observing episodic variations of organic aerosols, providing molecular level insights into formation and evolution of OA during winter haze episodes in urban atmosphere. While studying evolution processes, previous research

predominantly deploys Aerosol Mass Spectrometer, which relies on molecular fragments for differentiation of OA sources. In comparison, this study has a unique advantage in source tracking in using more source specific organic molecular markers. Our observations reveal notable diversity in OA transformations between haze episodes under influence of different air masses, providing measurement-based evidence in prioritizing control strategies for future air quality improvement.

2. Methods

2.1 Sampling site and online measurements

The winter campaign was conducted at the site of Shanghai Academy of Environmental Sciences (SAES) site (31°10′N,121°25′E) from 25th November 2019 to 23rd January 2020. Detailed descriptions of this urban site can be obtained in several published papers (Liu et al., 2021; Wang et al., 2020; He et al., 2020; S. Zhu et al., 2021). A comprehensive set of online instruments (Table 1) were operated on the roof of an eight-floor building (~25 m above ground) at SAES, including the TAG system (TAG, Aerodyne Research Inc). The measurement principle and operational procedure of the TAG system have been detailed in previous studies (He et al., 2020; Kreisberg et al., 2009; Wang et al., 2020; Williams et al., 2006; S. Zhu et al., 2021). In brief, the TAG system was operated with a time resolution of 2 hours. During the first hour, aerosol was collected at a flow of 10 L/min, and during the second hour, GC-MS analysis was performed. After sampling at room temperature and subsequent addition of 5 μL internal standard (IS) mixtures, the thermal desorption cell (CTD) was held at 45 °C for 2 min, then increased to 330 °C in 6 min, and held at 330 °C for 12 min. During this thermal desorption step, polar organic compound in $PM_{2.5}$ deposit on the CTD underwent in-situ derivatization under a helium stream saturated with derivatization agent N-methyl-N-(trimethylsilyl) trifluoroacetamide (MSTFA). Subsequently, the organic compounds were re-concentrated onto a focusing trap (FT) cooled by a fan. Afterwards, the CTD was purged with pure helium to vent the excess MSTFA and the FT was heated to 330°C to transfer the organic compounds into the valve-less injection (VLI) system, which employs a restrictive capillary tube to connect with the inlet of the gas chromatograph (GC). Then the GC/MS analysis started and concurrently, the next ambient sample was collected via the above-mentioned steps. In this study, a total of 98 polar and nonpolar organic compounds were identified and quantified (Text S1) and the full list is provided in Table S1. The detailed quality control measures and results for the TAG measurements have also been reported in S. Zhu et al. (2021) and given in section 2.2.1.

Additionally, multiple high-time-resolution instruments for the measurements of organic fragments in PM_1, major components and trace elements in $PM_{2.5}$, as well as gaseous and particulate pollutants were also available in this campaign (Table 1). The performance of AMS in measuring PM_1 organics during this field campaign has been reported in Huang et al. (2021) and its PMF analysis results are given in Figure S1. More detail descriptions of these instruments employed during the campaign have given in Text S1 and can also be referred to our previous studies (Qiao et al., 2014; Wang et al., 2013; S. Zhu et al., 2021). Meteorological parameters including temperature, relative humidity (RH), wind direction (WD), wind speed (WS) and solar radiation (RS) were measured concurrently at this site.

Table 1. Comprehensive online instruments adopted for this campaign.

Instrument	Parameters	Time resolution	Model (Manufacturer)
Thermal desorption Aerosol Gas chromatography-mass spectrometry system	Organic molecular markers in $PM_{2.5}$	2 hour	TAG (Aerodyne Research Inc., USA)

Monitor for AeRosols and Gases	Inorganic water-soluble ions (NO_3^-, SO_4^{2-}, Cl^-, NH_4^+, Na^+, Mg^{2+}, Ca^{2+}, K^+) in $PM_{2.5}$	1 hour	MARGA ADI 2080 (Applikon Analytical B.V., Switzerland)
Semi-continuous OC/EC analyzer	OC, EC in $PM_{2.5}$	1 hour	Model RT-4 (Sunset Laboratory, USA)
Online non-destructive X-ray fluorescence spectrometer (XRF)	15 trace elements (K, Ca, V, Cr, Mn, Fe, Ni, Cu, Zn, As, Se, Ba, Pb, Si, and S) in $PM_{2.5}$	1 hour	Xact® 625 Ambient Continuous Multi-metals Monitor (Cooper Environmental Services, USA)
Online beta attenuation particulate monitor	$PM_{2.5}$	1 min	FH 62 C14 series (Thermo Fisher Scientific Inc., USA)
NO_x monitor	NO, NO_2	1 min	Model 42i (Thermo Fisher Scientific Inc., USA)
O_3 monitor	O_3	1 min	Model EC9811 (Ecotech Inc., Australia)
Online gas chromatography systems equipped with flame ionization detector (GC‑FID)	C_2 - C_{12} VOCs in gas phase	30min	Chromato-sud airmoVOC C2-C6 #5250308 and airmoVOC C6-C12 #2260308, (Chromatotec, Bordeaux, France)
Aerosol mass spectrometer	Organics in PM_1	1 min	AMS (Aerodyne Research Inc., USA)

2.2 Data analysis

2.2.1 Data quality and control

A total of 638 valid samples were measured by TAG throughout the field campaign. A mixture of 20 deuterated compounds was added as internal standards in analysis of each sample and in calibration, to track and correct the changes in instrumental sensitivity. Table S1 lists the range and average concentrations of the 98 quantified organic compounds, together with their respective quantification ions and internal standards. For the ease of discussion, the 98 TAG-measured organic compounds are sorted into 18 compound groups in the following discussions, labeled as alkanes, hopanes, polycyclic aromatic hydrocarbons (PAHs), primary sugars (PSs), biomass burning tracers (BBtracers), unsaturated fatty acids (uFAs), saturated fatty acids (sFAs), aromatic polycarboxylic acids (Ar-PCAs), nitro-aromatic compounds (NACs), C_9 acids, C_{6-8} hydroxyl dicarboxylic acids (H_hDCAs), C_{6-8} dicarboxylic acids (H_DCAs), C_{3-5} hydroxyl dicarboxylic acids (L_hDCAs), C_{3-5} dicarboxylic acids (L_DCAs), phthalic acid (Pht), 2,3-dihydroxy-4-oxopentanoic acid (DHOPA), β-caryophyllene tracers (βCaryT) and α-pinene tracers (αPinT), considering both compound structures and commonality in source origins. Molecules lumped into the same group normally show correlations with each other with R_p higher than 0.6 (Figure S2). We further evaluated the quality of hourly dataset by conducting multiple cross-comparisons among independent measurements, of which scatter correlation plots are illustrated in Figure S3. For example, the summed mass of 98 TAG-measured organic molecules is well correlated with OC measured by OC/EC analyzer ($R^2 = 0.73$) and total organics measured by AMS ($R^2 = 0.74$). TAG-measured hopanes and fatty acids are well-correlated with the hydrocarbon-like OA (HOA, $R^2 = 0.60$) and cooking OA (COA, $R^2 = 0.74$) resolved from the mass spectra by AMS, respectively, reflecting vehicular emissions (VE) and cooking activities as their respective common source. And those secondary organic molecules (e.g., pinic acid, DHOPA, phthalic acid, DCAs, and hDCAs) measured by TAG showed moderate to strong correlations ($R^2 = 0.21\sim0.68$) with nitrate, sulfate measured by MARGA and secondary source factors (e.g., MO-OOA, LO-OOA) derived from AMS. Besides, the inorganic ions (NO_3^-, SO_4^{2-}, NH_4^+) measured by AMS fairly well correlated with those measured by MARGA ($R^2 = 0.59\sim0.79$). The summed secondary source factors derived from AMS also showed strong correlations ($R^2 = 0.87$) with SOM estimated by OC/EC ratio method, and its summed primary source factors correlated well with estimated POM ($R^2 = 0.44$). Overall, the data consistency checks indicate that the TAG system and other online instruments have provided good quality measurements.

2.2.2 Estimation of primary and secondary organic aerosol mass concentrations

OC in the ambient $PM_{2.5}$ can be apportioned into primary OC (POC) and secondary OC (SOC) according to their source

origins. As it is analytically infeasible for direct measurement of POC and SOC, an estimation method based on OC/EC ratio is widely adopted (Castro et al., 1999; Turpin and Huntzicker, 1995). Specifically, EC serves as a tracer to track the portion of co-emitted POC and the following equations are used to calculate POC and SOC:

$$POC = EC \times (OC/EC)_{pri} \tag{1}$$

$$SOC = OC - POC \tag{2}$$

where OC and EC are the measured hourly concentrations of OC and EC, and $(OC/EC)_{pri}$ is the average OC-to-EC ratio from primary emission sources. In this study, the minimum OC/EC ratio of 1.5 during the campaign was adopted to represent $(OC/EC)_{pri}$ (Lim and Turpin, 2002). This value fell in the range reported in other studies (1.4~1.9) for estimating POC and SOC concentrations in Shanghai (Wang et al., 2016; Yao et al., 2020; Zhao et al., 2015). Subsequently, primary organic matter (POM) and secondary organic matter (SOM) were calculated from POC and SOC by multiplying conversion factors of 1.4 and 2.0, respectively. The multipliers were previously reported in W. Zhu et al. (2021) based on the 2016-2017 AMS data measured at the same site.

2.3 Clustering analysis and concentration weighted trajectory (CWT)

Backward trajectories for air masses arriving at the observation site and their clustering analysis were calculated every hour by HYSPLIT software (http://ready.arl.noaa.gov/HYSPLIT.php) with 6-hour archived GDAS (Global Data Assimilation System) data. Based on the change in total spatial dissimilarity (TSV) (Figure S4) and variations of $PM_{2.5}$ chemical composition under each cluster (Figure S5), an optimal solution of four clusters (Figure S5), representing marine, local, YRD transported and long-range transported air masses, was determined. The information derived from HYSPLIT was then used to determine the potential source areas for $PM_{2.5}$ under the influence of different air mass clusters and the results are illustrated by concentration weighted trajectory (CWT) approach with the adoption of ZeFir software (Petit et al., 2017). More detailed description of these analyses is given in Text S2.

3. Results and Discussion

3.1 General descriptions

Figure 1 shows the time series of meteorological parameters, gaseous pollutants, and $PM_{2.5}$ and its chemical components during the campaign. The average $PM_{2.5}$ mass loading was 49.9 ± 36.9, μg/m³ and significant hour-to-hour variation was recorded. $PM_{2.5}$ episodes were identified to be periods of hourly concentrations exceeding 35 μg/m³ and durations over 20 hours. A total of nine $PM_{2.5}$ episodes (EP#1 – EP#9) thus emerged throughout the study period and are individually labeled in Figure 1. Among them, EP#1, EP#7 and EP#8, which lasted from 31 to 105 hours, were categorized into "transport episodes" on the basis that their trajectories with high particle concentrations originated from Shandong province and passed over YRD region before reaching Shanghai (Figure 2a). EP#3, EP#4 and EP#6 were categorized as "local episodes", as they were characterized by significantly lower moving speed of polluted air parcels circling around Shanghai (Figure 2a). Compared with transport episodes, the durations of local episodes were normally much shorter, ranging from 21 to 38 hours. EP#2, #5 and #9, each lasting over 4 days with high $PM_{2.5}$ concentrations originated from both the YRD region and local areas (Figure 2a), were thus termed as "mixed-influence episodes". The remainder days were classified as non-episodic periods, characterized by notably lower concentrations of most ambient pollutants (e.g., $PM_{2.5}$, NO_x, VOCs). Consistent with previous studies (Li et al., 2019; Wang et al., 2014b; Wei et al., 2019), the occurrences of haze episodes in Shanghai during wintertime were associated with air parcels originating from the YRD region or local areas under stagnant meteorological conditions,

while the clean periods were characterized by prevailing air masses that were transported long-range from Mongolia or clean marine areas. These long-range transported air masses were associated with higher wind speed (WS > 4 m/s), thus favoring the diffusion and dilution of air pollutants. More detailed statistics related to the average values of meteorological parameters, ambient pollutants, $PM_{2.5}$ major components and diagnostic ratios during individual episode categories and non-episodic periods are summarized in Table 2.

Among the three types of episodes, $PM_{2.5}$ concentration showed the highest average level during transport episodes (83.5 $\pm$ 37.0 µg/m^3) with hourly concentration fluctuating from 32 to 178 µg/m^3, followed by the mixed-influence episodes (78.0 $\pm$ 29.5 µg/m^3) and local episodes (62.4 $\pm$ 25.3 µg/m^3) (Table 2). During the transport and mixed-influence episodes, high concentrations of $PM_{2.5}$ were observed along with relatively higher concentration of O_3 under lower level of RH (< 70%) and higher intensity of solar radiance (RS > 80 W/m^2). Local episodes generally occurred with a notable drop of WS (2.3 $\pm$ 1.4 m/s) and relatively higher level of RH (83.7 $\pm$ 9.3%). Apparently, the stagnant meteorological conditions were favorable for the accumulation of pollutants from local emissions. Significant higher levels of NO_x (98.2 $\pm$ 46.6 ppbv) and volatile organic compounds (VOCs) (74.5 $\pm$ 31.5 ppbv), as well as NO/NO_2 (1.30 $\pm$ 1.09) and toluene/benzene (T/B, 3.8 $\pm$ 1.7) ratios, were also observed during local episodes, reflecting their origin of local vehicular and combustion sources with less influence from aging processes.
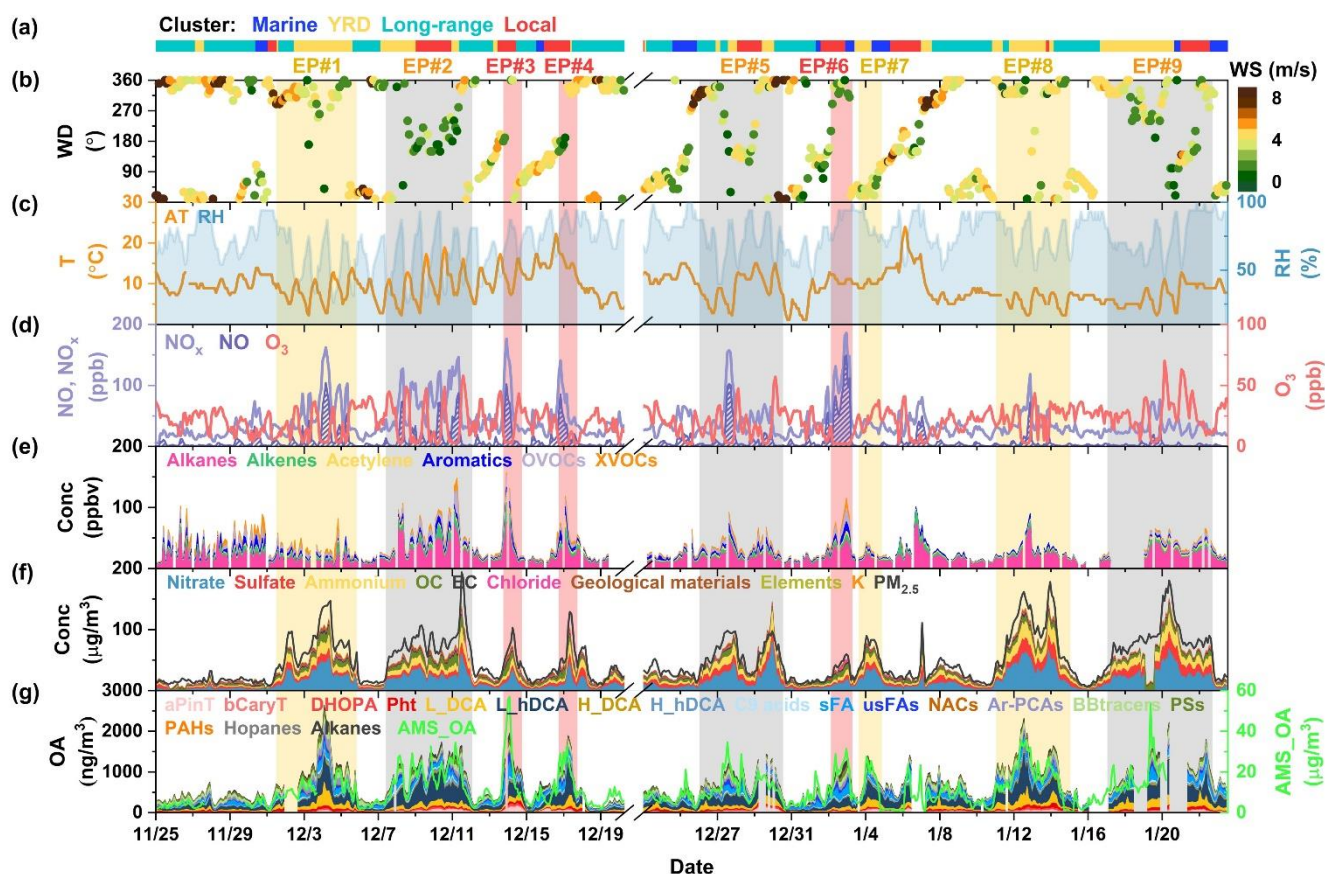
Figure 1. Time series of (a) air mass clusters; (b) wind direction (WD), wind speed (WS); (c) temperature (T), relative humidity (RH); (d) NO, NO_x, O_3; (e) VOCs measured by GC-MS (see Table S2 for the VOC groups and individual VOCs); (f) major components of $PM_{2.5}$ and total $PM_{2.5}$ (dark line); and (g) organic molecular groups in $PM_{2.5}$ measured by TAG and total OA (green line) in PM_1 measured by AMS during the campaign. The concentration of geological materials was calculated to be 2.49[Si] + 1.63[Ca] + 2.42[Fe], and concentration of elements was calculated as the sum of V, Cr, Mn, Ni, Cu, Zn, As, Se, Ba, and Pb. The nine episodic events were shaded in yellow, grey and

190 red, representing transport, mixed-influence and local episodes, respectively.

Table 2. Summary of meteorological parameters, ambient pollutants, PM$_{2.5}$ major components and diagnostic ratios for different types of episodes and non-episodic periods.

Parameters	Local episodes	Mixed-influence episodes	Transport episodes	Non-episodic periods
	EP#3, #4, #6	EP#2, #5, #9	EP#1, #7, #8	/
Meteorological factors				
RH (%)	83.7 ± 9.3	69.2 ± 17.8	67.8 ± 17.4	76.8 ± 13.7
WS (m/s)	2.3 ± 1.4	3.1 ± 2.1	3.4 ± 1.7	4.4 ± 2.0
RS (W/m^2)	41.0 ± 110.2	95.9 ± 167.4	86.0 ± 151.9	60.7 ± 125.3
Ambient pollutants				
PM$_{2.5}$ (μg/m^3)	62.4 ± 25.3	78.0 ± 29.5	83.5 ± 37.0	22.6 ± 12.2
NO$_x$ (ppbv)	98.2 ± 46.6	48.7 ± 32.2	46.3 ± 30.1	29.6 ± 14.1
O$_3$ (ppbv)	5.5 ± 7.2	21.5 ± 15.9	19.7 ± 11.5	20.9 ± 9.6
VOCs (ppbv)	74.5 ± 31.5	48.8 ± 24.6	30.3 ± 13.8	27.8 ± 17.8
PM$_{2.5}$ composition				
Nitrate (%)	24.8 ± 6.7	33.1 ± 8.6	34.6 ± 6.6	21.2 ± 7.8
Sulfate (%)	10.4 ± 2.5	14.8 ± 6.0	12.3 ± 3.8	17.7 ± 5.9
Ammonium (%)	11.7 ± 2.2	15.3 ± 3.6	14.8 ± 2.2	12.4 ± 3.4
SOM (%)	26.5 ± 10.6	15.8 ± 5.4	13.3 ± 3.8	20.5 ± 8.3
POM (%)	6.6 ± 2.8	3.1 ± 1.1	3.4 ± 1.0	5.4 ± 2.5
Others (%)	20.0 ± 13.3	17.9 ± 15.0	21.6 ± 9.2	22.8 ± 15.3
Ratios				
NO/NO$_2$	1.30 ± 1.09	0.26 ± 0.36	0.26 ± 0.35	0.19 ± 0.21
NO$_3^-$/SO$_4^{2-}$	2.55 ± 1.00	2.60 ± 1.12	3.07 ± 1.00	1.31 ± 0.63
Toluene/Benzene	3.8 ± 1.7	1.8 ± 1.1	1.7 ± 1.2	2.2 ± 1.6

Figure 2 (b) shows chemical compositions in PM$_{2.5}$ and mass percentages of SOM during the nine episodes as well as
195 non-episodic periods, and Figure 2 (c) compares the mass increment ratios and mass percentages of SOM with that of combined secondary inorganic aerosols (SIA, including NO$_3^-$, SO$_4^{2-}$ and NH$_4^+$) among different episodes. In general, secondary species (e.g., NO$_3^-$, SO$_4^{2-}$, NH$_4^+$, SOM) constituted the largest fraction of PM$_{2.5}$ during both polluted (68%-86%) and clean (75%) periods, yet the composition was substantially different. Mass contributions of secondary inorganic aerosol to PM$_{2.5}$ were much higher during transport episodes and mixed-influence episodes. Especially for nitrate, which accounted for 31%-40% of PM$_{2.5}$
200 average concentration during transport episodes versus 23%-28% of PM$_{2.5}$ mass concentration during local episodes and non-episodic days. In contrast, SOM took up a more prominent portion in PM$_{2.5}$ during local episodes ranging from 22% to 27%. The highest portion of SOM (27%) occurred during the local episode EP#6, and this fraction even exceeded nitrate (26%).

While SIA had comparable percentage contributions to PM$_{2.5}$ during all episodes (46%-72%), higher mass incrementation of SOM was observed during local haze episodes with a ratio of 2.8-3.9 to non-episodic periods, highlighting the importance
205 of secondary organic aerosol formation in local PM$_{2.5}$ pollution. Indeed, primary species (e.g., POM, EC, potassium, chloride, geological material matters and other trace elements) also showed noticeable increases with summed contributions up to 29% during local episodes, while their percent contributions during the transport and mixed-influence episodes were in the range of 8-14%. The higher proportions of primary species together with significantly higher values of NO/NO$_2$ and T/B ratios indicate that local PM$_{2.5}$ episodes in Shanghai were largely influenced by freshly emitted primary pollutants in the local areas.
210 These results suggest largely different sources and chemical processing of PM$_{2.5}$ formation under different haze types.
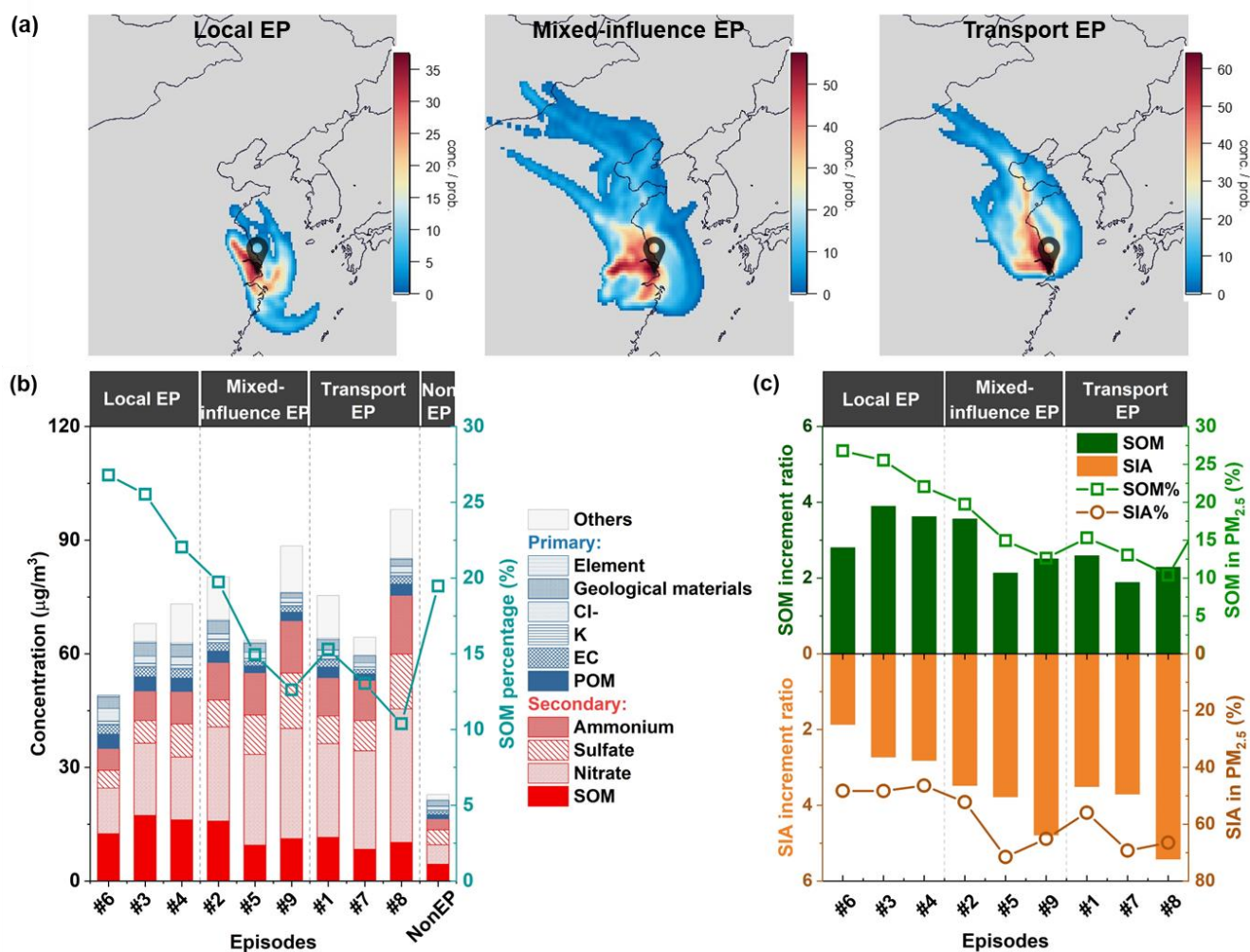
Figure 2. (a) Concentration weighted trajectory (CWT) maps for $PM_{2.5}$ (the droplet icon in the maps represents the location of the observation site) and (b) its chemical compositions during different episodes; (c) comparisons of mass increment ratios of SOM and combined SIA during different episodes in reference to non-episodic periods. Mass increment ratio close to 1 indicates no obvious increment.

3.2 Characteristics of organic compound groups during haze episodes

3.2.1 Major classes of organic compounds in $PM_{2.5}$

The average concentration of total 98 organic compounds measured by TAG system during the campaign was 809 ± 499 ng/m^3. Among the quantified OA markers, the L_hDCAs group exhibited the highest concentration (264 ± 187 ng/m^3), which was dozens to hundreds of times higher than those of the other groups. Malic acid and glyceric acid were the main components of L_hDCAs, the former of which was also the most abundant individual compound among all 98 measured compounds. The average concentrations of malic acid and glyceric acid during the campaign were 156 ± 112 ng/m^3 and 54 ± 44 ng/m^3, respectively. These levels were at the same magnitude as those observed at urban sites in Hong Kong (Hu et al., 2008; Hu et al., 2013; Lyu et al., 2020). The concentration level of L_DCAs was only second to that of L_hDCAs with an average value of 95 ± 83 ng/m^3. The high mass concentrations and proportions of these highly oxidized organic molecules (L_hDCAs and L_DCAs) indicates that aerosols measured at this site were frequently aged. Of comparable concentration to L_DCAs was saturated fatty acids (sFAs) (93 ± 80 ng/m^3), signaling the influence of cooking activities on $PM_{2.5}$ at this urban site. As listed in Table S1, BBtracers, which are specific organic molecular tracers for biomass burning, had an abundance level of (72 ± 41

ng/m^3). Ar-PCAs were indicators for secondary products of biomass burning emissions (He et al., 2018; Schauer et al., 2002). The sum concentration of Ar-PCAs was 40 ± 33 ng/m^3 during the campaign. Ar-PCAs were well correlated with both BBtracers (Figure S2) and secondary inorganic ions (Figure S6). The relatively high concentrations of BBtracers and Ar-PCAs among the 18 groups implies that biomass burning activities during wintertime still persisted and transported to urban Shanghai despite the prohibition of field fires implemented in recent years. The unambiguous molecular information offered by the TAG system also enables us to interpret OA aging processes through specific SOA tracers and their formation chemistry established in controlled chamber experiments. Among the SOA groups, L_DCAs and L_hDCAs were regarded as aging SOA tracers since their formations require multiple oxidation steps in the chamber experiments (Ervens et al., 2004; Yang et al., 2008). While for some other SOA tracers such as pinic acid and pinonic acid, which were classified into αPinT, they were interpreted as fresh SOA since they have been confirmed by a number of chamber studies that are early generation SOA products of α-pinene ozonolysis (Kristensen et al., 2014; Ma et al., 2008; Szmigielski et al., 2007). The strong correlations of L_DCAs and L_hDCAs with more-oxidized organic aerosol (MO-OOA) derived from AMS measurements and αPinT with less-oxidized organic aerosol (LO-OOA) (Figure S3) further supports our interpretations of aging and non-aging SOA.

3.2.2 Comparison of OA variations between local and transport episodes

Table 3 reveals distinct concentration levels of organic markers for different air pollution types and Figure S7 shows their mass percentages. In general, the proportions of organic molecular groups in PM$_{2.5}$ differed among different episodic types. During local episodes, the TAG-measured OA (average 1409 ng/m^3) was characterized by sizable contributions from primary and secondary anthropogenic organic molecules, including alkanes, PAHs, hopanes, uFAs, sFAs, C$_9$ acids, DHOPA, pht, which contributed 47% of the mean mass concentration. On the contrary, the TAG-measured OA during transport episodes (average: 1164 ng/m^3) was dominated by secondary organic molecular groups such as L_DCAs (167 ± 103 ng/m^3) and L_hDCAs (358 ± 176 ng/m^3), when examining the relative proportion of primary and secondary organic molecules. These two groups have been highlighted as later oxidation products of primary precursors with a wide range of sources, and they made up 45% of the mean mass concentration. Despite the notably lower contributions (32%) from the sum of primary organic molecules (sFAs, uFAs, BBtracers, PSs, alkanes, PAHs and hopanes) during transport episodes, the average proportion of BBtracers in TAG-measured OA ascended from 5% during local episodes to 10% during transport episodes. Higher contributions from Ar-PACs and NACs were also observed during the mixed-influence and the transport episodes compared with the local episodes, suggesting that biomass burning played an important role in the accumulation of transported PM$_{2.5}$. Overall, TAG-measured OA was over 20% more abundant in mass concentration in the atmosphere during local episodes compared to the mixed-influence episodes and the transport episodes.

Table 3. Mean Levels of TAG-measured organic molecular groups and total OA during different types of PM$_{2.5}$ pollution episodes.

Organic molecular groups* (ng/m^3)	Local episodes EP#3, #4, #6	Mixed-influence episodes EP#2, #5, #9	Transport episodes EP#1, #7, #8	Non-episodic periods /
αPinT	75.9 ± 24.9	41.6 ± 26.1	39.3 ± 18.9	15.4 ± 15.3
βCaryT	2.97 ± 0.85	1.68 ± 0.83	2.12 ± 1.03	0.79 ± 0.80
DHOPA	45.6 ± 12.6	20.9 ± 11.3	17.9 ± 11.3	5.2 ± 4.9
Pht	61.0 ± 22.4	32.0 ± 20.2	48.4 ± 24.3	17.7 ± 14.2
L_DCAs	96.4 ± 46.4	154.6 ± 70.7	166.6 ± 102.7	42.5 ± 29.3
L_hDCAs	304.8 ± 120.4	406.4 ± 197.2	357.7 ± 176.1	157.5 ± 108.7
H_DCAs	43.3 ± 18.3	25.2 ± 12.7	19.3 ± 12.4	7.6 ± 5.6
H_hDCAs	57.0 ± 22.6	40.6 ± 22.8	37.1 ± 23.5	11.4 ± 11.7
C9 acids	40.9 ± 16.5	27.4 ± 18.3	17.6 ± 10.3	9.6 ± 7.6
sFAs	292.3 ± 145.9	110.2 ± 59.7	109.7 ± 57.1	60.0 ± 47.4

uFAs	101.3 ± 81.8	35.4 ± 32.3	28.0 ± 26.2	18.5 ± 21.1
Ar-PCAs	39.2 ± 15.3	53.3 ± 30.9	77.7 ± 40.0	22.2 ± 16.1
NACs	6.14 ± 3.06	10.3 ± 7.12	9.17 ± 5.39	2.49 ± 2.51
BBtracers	73.3 ± 28.1	81.8 ± 33.5	118.4 ± 40.4	51.3 ± 28.9
PSs	42.9 ± 15.0	42.1 ± 21.6	58.8 ± 36.9	25.8 ± 18.8
Alkanes	110.8 ± 47.5	44.6 ± 25.5	47.7 ± 25.2	24.3 ± 17.5
PAHs	12.5 ± 7.19	6.01 ± 2.61	7.33 ± 3.55	2.89 ± 1.65
Hopanes	2.81 ± 1.15	1.34 ± 0.97	1.34 ± 0.88	0.73 ± 0.46
TAG-measured OA	1409.0 ± 389.5	1135.5 ± 424.0	1164.1 ± 469.4	476.1 ± 241.9

* Full names of the listed organic molecular groups and their included compounds can be found in section 2.2.1 and Table S1.

Figure 3 compares the mass abundances of four groups of species between episodic periods and non-episodic periods, including (1) individual TAG-measured organic molecules in total TAG-measured OA, (2) major components in $PM_{2.5}$, (3) subgroups of OA in PM_1 as resolved by PMF analysis of the AMS data, and (4) single VOC out of the sum of a select set of VOCs, OVOCs, and XVOCs, in which OVOCs denotes oxygenated volatile organic compounds and XVOCs refers to halogenated VOCs. Species positioned above the 1:1 line indicate enhancement during episodes. The results show that different sets of species were enhanced during the three episode types. During local episodes, the OA mass increments were mainly attributable to those from vehicular emissions (e.g., hopanes) and cooking activities (e.g, fatty acids). The mass percentages of primary vehicular-emitted tracers, such as PAHs, alkanes and hopanes increased from 0.6%, 5.1%, and 0.1% in total TAG-measured OA during clean periods to 0.9%, 7.9% and 0.2% during local episodes, respectively. Saturated and unsaturated fatty acids showed a drastic increase from 16% (non-episodes) to 28% (local episodes). Other inorganic species, including EC, chloride, and elements also exhibited higher mass proportions in $PM_{2.5}$ during local episodes, indicating that local primary emissions such as vehicle exhaust and cooking played an important role in the formation of hazes. In addition to these primary components, vehicular and industrial source-related secondary compounds, such as DHOPA and phthalic acid also showed elevated contributions in the total TAG-measured OA with percentages of 3.2% and 4.3%, respectively, during local episodes. These results suggest that local anthropogenic sources were major contributors to elevating $PM_{2.5}$ pollution. Note that unlike sFAs and uFAs, the C_9 acids, which were mainly ozone oxidation products of uFAs, did not show drastic increase during local episodes in their mass proportions in TAG-measured OA and AMS-derived OCOA in PM_1. This could be explained by the significantly higher NO_x concentrations and NO/NO_2 mass ratios during local episodes (Table 2), which likely suppressed O_3 chemistry to a large extent. This hypothesis is also supported by the smaller increases in mass concentrations of other ozonolysis SOA products such as αPinT and βCaryT, which increased by 393% and 276% during local episodes in reference to non-episodic periods, respectively (Table 2). In comparison, DHOPA, which is a typical SOA product of monoaromatics reacting with OH radicals, showed a much more drastic increase of 777% in the mass concentration during local episodes (Table 2). Such contrasts between SOA products from OH-initiated vs O_3-initiated oxidation pathways appear to suggest that SOA formed during local episodes were more influenced by pathways other than ozonolysis (e.g., OH oxidation).

Different from local episodes, the majority of primary components during mixed-influence and transport episodes decreased in mass percentage compared with non-episodic periods. The mass percentages of sFAs, uFAs, alkanes, and hopanes in total TAG-measured OA decreased to 9.4%, 2.4%, 4.1% and 0.11% during transport episodes from 12.6%, 3.9%, 5.1%, and 0.15% during clean periods, respectively. Exceptions were BBtracers, PSs, and PAHs, which exhibited comparable proportions during transport episodes and non-episodic periods. Similarly, primary inorganic species and AMS-derived primary OAs in PM_1 also decreased in mass abundance during the mixed-influence and transport episodes. On the other hand, mass proportions of most secondary organic molecular groups elevated, with the summed values reaching 68% during transport episodes and 72% during mixed-influence episodes, which were remarkably higher than 55% during local episodes and 61% during non-episodic periods. Noticeably, those TAG-measured organic molecules that have increased in mass percentages during local

episodes were generally less-oxidized compared with that during mixed-influence and transport episodes, in consistent with the observation that transported PM$_1$ contained higher proportions of MO-OOA while LO-OOA accounted for more PM$_1$ mass during local episodes (Figure S7). In other words, the higher mass concentrations and mass percentages of OA in PM$_{2.5}$ during local episodes were mainly contributed by primary OA and less-oxidized SOA, while aerosols during the mixed-influence and transport episodes were generally influenced by more aged SOA.
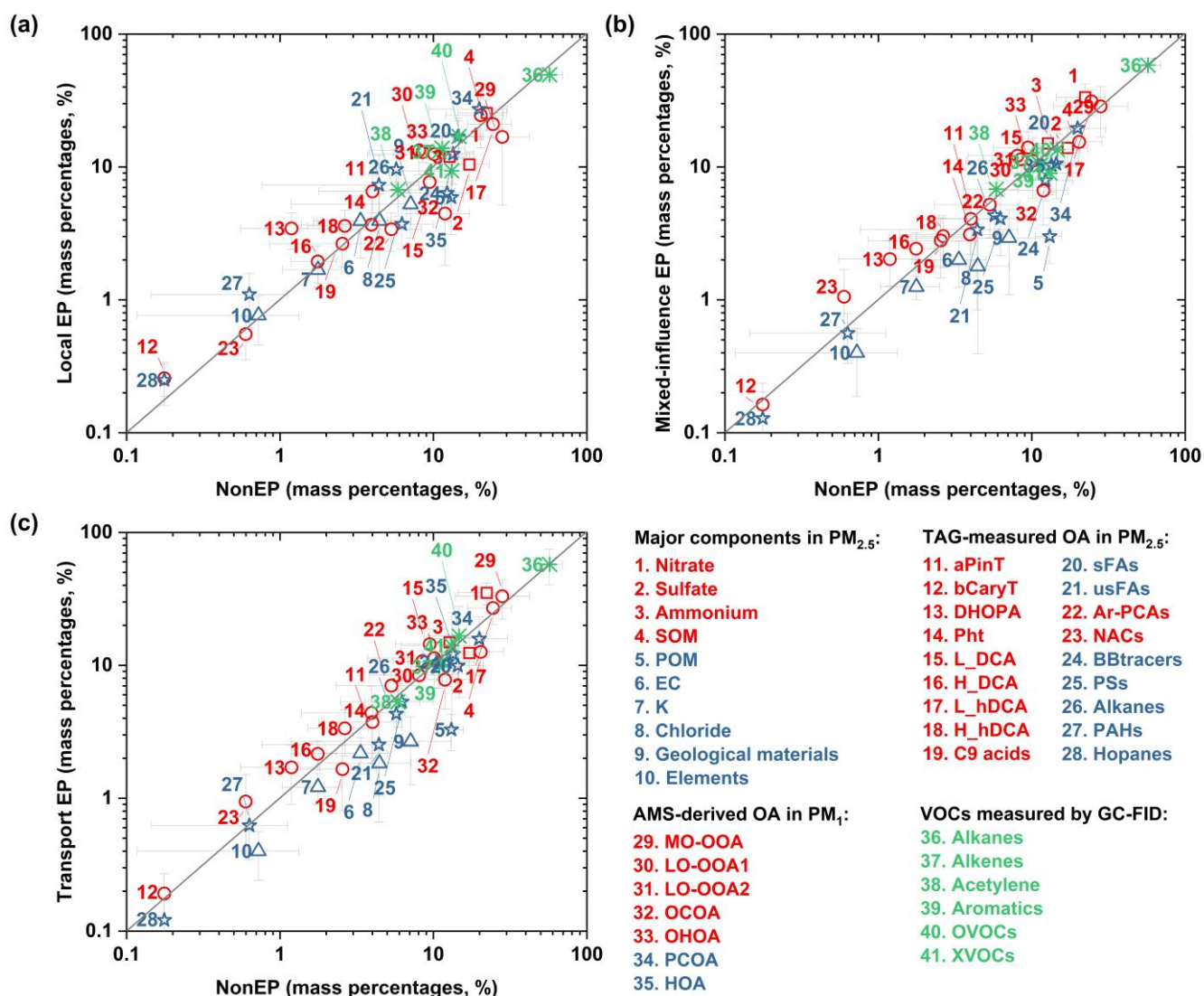
Figure 3. Comparison of measured VOCs and PM components in mass percentages between (a) local episodes, (b) mixed-influence episodes, and (c) transport episodes against non-episode periods. The comparison plots cover four groups of mass percentages, namely, individual organic molecule in total TAG-measured OA, major components in PM$_{2.5}$, sub-categories of bulk OA in PM$_1$, and single VOC in the sum of a select group of VOCs. Data are grouped by colors and symbols, with red open circles representing secondary origins, blue open triangles representing primary origins, green asterisks donating VOCs (e.g., alkanes, alkenes, acetylene, aromatics), OVOCs, and XVOCs in total VOCs. The measured VOC species included in alkanes, alkenes, acetylene, aromatics, OVOCs are given in Table S2. Detail information related to the identification and quantification of AMS-derived OA subgroups in PM$_1$ can be referred to Huang et al. (2021). Data located above the 1:1 line indicate an increase in respective mass proportions during episodes as compared with non-episodic periods.

3.3 Variations of secondary organic molecular tracers during episodes

3.3.1 2,3-dihydroxy-4-oxopentanoic acid (DHOPA) and aromatic SOA estimates

As discussed in the previous sections, DHOPA in TAG-measured OA had remarkable elevation in both absolute mass concentration and mass proportion during local episodes. Correlation analyses of DHOPA versus other source tracers during different episodes were performed and shown in Figure S9. The moderate to strong correlations between DHOPA and estimated SOM during all nine episodes reaffirmed the secondary nature of DHOPA. DHOPA played a larger role in SOA formation during local episodes in comparison with the mixed-influence and transport episodes, as suggested by the generally higher R^2 (0.55~0.75) and slopes (1.3~1.6) during local episodes.

It is also informative to examine the correlations of DHOPA with primary tracers. DHOPA had strong correlations with hopanes during local episodes (R^2: 0.62 to 0.82), but the correlations were much weaker during transport episodes (R^2: 0.34~0.56) and nearly negligible during mixed-influence episodes (R^2: 0.00~0.28). In contrast, DHOPA had stronger correlations with PAHs (e.g., BbF, BkF, BaF, BeP, BaP, IcdP, BghiP) (R^2: 0.53~0.72) during transport episodes, which was likely related to coal combustion. Such differences could be explained as a result of differing aromatic precursor sources for DHOPA among local versus transport episodes, with the dominating precursor sources being the vehicular emissions during local episodes versus sources such as coal combustion and biomass burning under the influence of transported air.

Taking advantage of the DHOPA data, we used a modified tracer-based method proposed by Gao et al. (2019) and Zhang et al. (2021a) to estimate aromatic SOA from ambient DHOPA measurements with gas-particle partitioning effects taken into consideration. The aromatic SOA could be viewed to consist of (1) semi-volatile aromatic SOA (SemiASOA) which is formed via gas-particle partitioning processes, and (2) more-oxidized aromatic SOA (MoASOA) that is associated with later generation products (e.g., oligomers and dicarbonyl compounds). Although a number of monoaromatics can form DHOPA, only toluene and xylenes were included in the SemiASOA estimation due to their predominant presence in urban area. The well estimated hourly DHOPA values further confirmed this. The mass yield coefficients of toluene and xylenes under high NO_x conditions were adopted from previous chamber experiments (Al-Naiema et al., 2020) and more details about this estimation method are provided in Text S3.

In general, a significant fraction (62%) of DHOPA was oxidized from m/p-xylenes through high-NO_x pathways during wintertime in Shanghai, regardless of episodic or non-episodic periods. Toluene only accounted for 38% of DHOPA mass concentration in average under high NO_x conditions (Figure S12). Several previous studies have also verified that it is incorrect to attribute all DHOPA-based aromatic SOA estimation to toluene and xylenes can be a more predominant precursor in aromatic SOA formation (Al-Naiema et al., 2020; Ma et al., 2018; Zhang et al., 2021b).

Comparing the contributions to total SOA from DHOPA-based semi-volatile aromatic SOA (SemiASOA), more-oxidized aromatic SOA (MoASOA) and SOA produced from precursors other than monoaromatic hydrocarbons (NonASOA) between episodic events and non-episodic periods as shown in Figure 4, drastic elevation in contributions from aromatic SOA were observed during episodic events. During non-episodic periods, aromatic SOA constituted around 21% of total SOA in wintertime in Shanghai, while this value rose to 32%~44% during episodic events. The mass contributions from aromatic SOA also increased from 0.94 μg/m³ during non-episodic periods to 3.3 ~ 7.5 μg/m³ during episodic events. This enhancement of SOA formation during episodes emphasizes the importance of controlling aromatic precursors for mitigating PM$_{2.5}$ pollution in a megacity like Shanghai. Especially during local episodes, considerable benefits with average 38% reduction in SOA can be expected to obtain if mono-aromatic VOCs are effectively controlled.

Among the nine episodes, notably higher contributions from SemiASOA were observed in local episodes, which constituted 17% of total SOA in average. Relatively lower contributions (7% -14%) from SemiASOA and higher fractions (24% -32%) of oligomers and dicarbonyl compounds (MoSOA) in total SOA were found during mixed-influence and transport

episodes. This suggests that SOA formed from aromatic hydrocarbons during mixed-influence and transport episodes generally contained more highly oxidized organic products compared with local episodes, which is in consistent with the observation as stated in section 3.2.
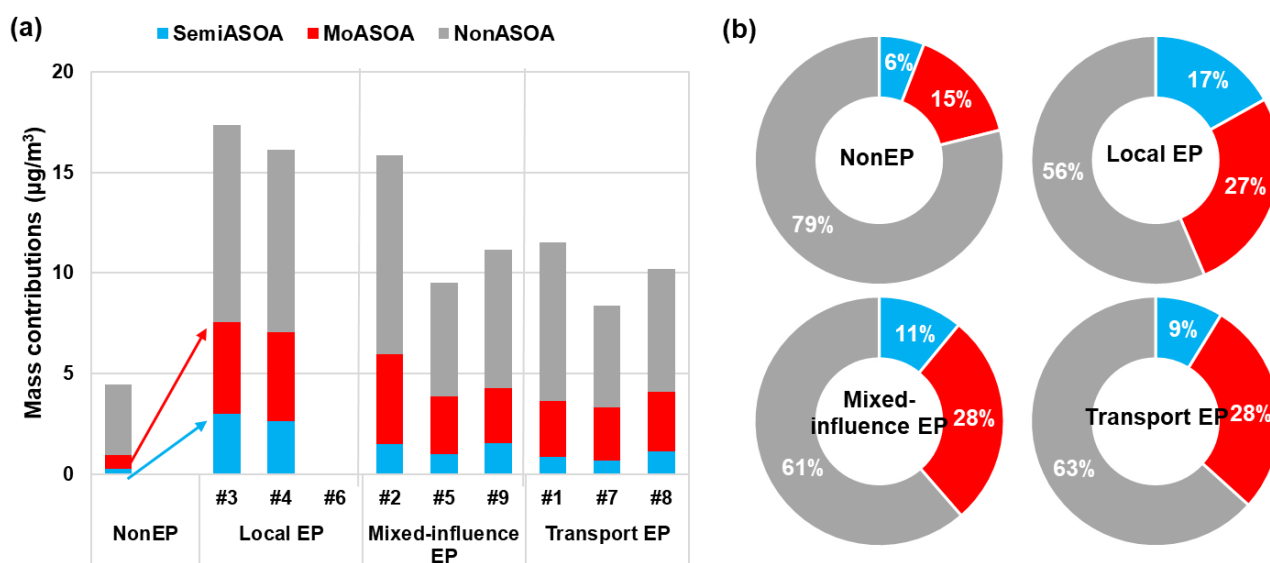
Figure 4. Predicted (a) mass contributions and (b) percentage contributions to total SOA from semi-volatile aromatic SOA (SemiASOA), more oxidized aromatic SOA (MoASOA) and SOA products oxidized from precursors other than aromatics (NonASOA) during episodic events and non-episodic periods. MoASOA here was calculated by subtracting SemiASOA from TotalASOA and NonASOA was estimated by subtracting TotalASOA from SOM which was calculated based on OC/EC ratio method.

3.3.2 Nitro-aromatic compounds (NACs)

Both primary emissions from combustion sources and nitration of aromatic hydrocarbons (e.g., benzene and toluene) are major sources of NACs in the atmosphere (Li et al., 2020; Wang et al., 2019; Yan et al., 2017). NACs measured in this study displayed moderate to strong correlations with SOM during all episodic events (Figure S13), implying that they were likely secondarily formed from aromatic hydrocarbons. Figure 5 shows the evolution of NACs with the increase concentrations of their VOC precursors during different episodes. During the whole campaign, benzene varied in the range of 0.0-1.9 ppb while toluene varied in the range of 0.1-7.1 ppb. In general, NACs concentrations ascended with the increasing of toluene and benzene during all episodic events. During local episodes, NACs displayed a linear growth with the elevation of toluene concentrations, while they did not further increase with benzene concentrations when benzene concentrations were higher than 1.5 ppb (Figure 5a, d). In comparison, NACs exhibited a linear increasing trend with benzene concentrations during the entire concentration range of 0.0-1.9 ppb while the linear correlation of NACs with toluene ceased when toluene was higher than ~3.5 ppb during mixed-influence episodes or ~2.5 ppb during transport episodes (Figure 5e, f). Toluene is a more reactive aromatic compound and more abundantly emitted from vehicular sources. As such, it is likely that toluene was a more predominant precursor in forming NACs during local episodes. Yet during mixed-influence and transport episodes, benzene was a more dominant aromatic hydrocarbon precursor for NACs due to its relatively stable chemical structure and higher influences from coal combustion and biomass burning associated with air masses from north China.

Figure S13 further confirmed that NACs concentrations during transport episodes were largely impacted by biomass burning emissions. Hourly concentrations of NACs showed strong correlations with organic tracers indicative of biomass burning (BBtracers) with R^2 higher than 0.64 during transport episodes, while the correlation coefficients dropped to 0.30

during local episodes. Such results suggested that biomass burning was a major source of NACs in Shanghai during transport episodes and likely had sizeable influence during local episodes. The stronger correlations between NACs and SOM with higher values of slopes during mixed-influence and transport episodes also suggested that NACs played a more important role in SOA formation during mixed-influence and transport episodes.
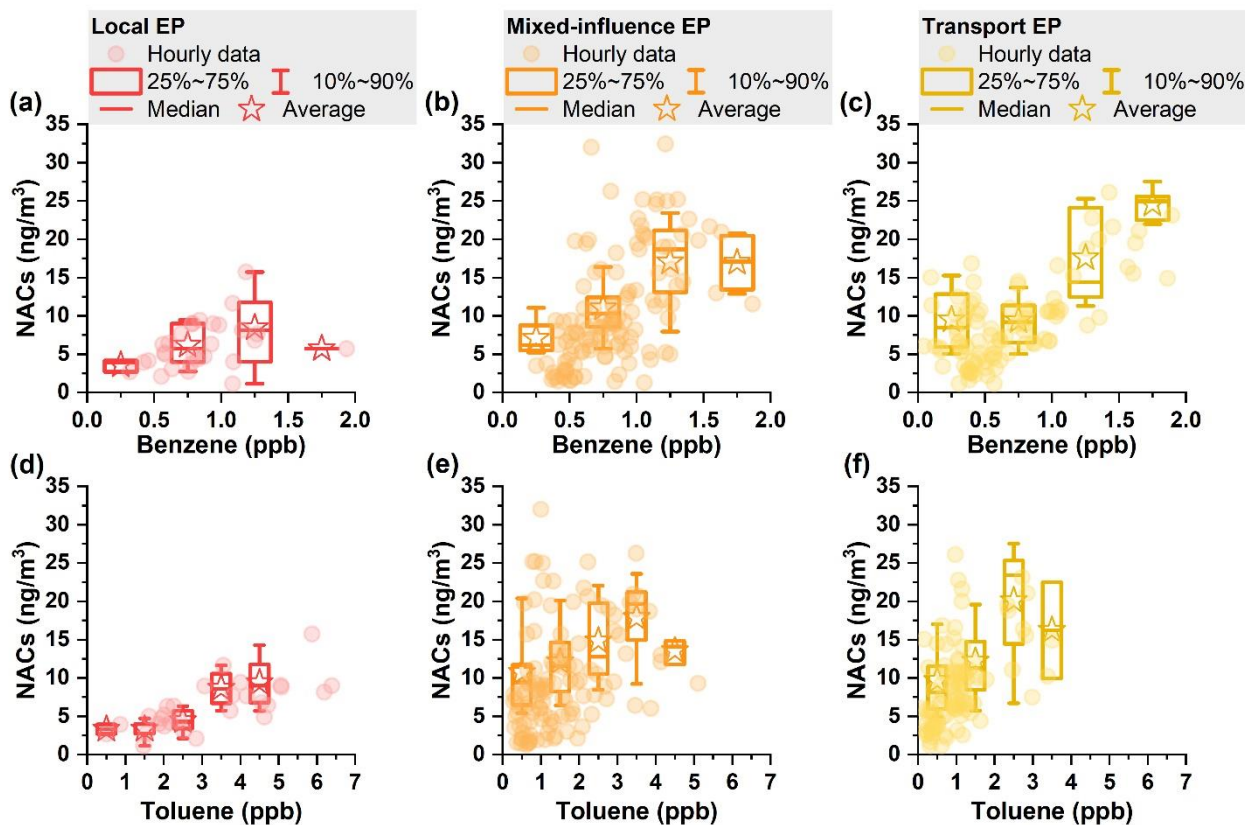
Figure 5. Concentrations of NACs as a function of benzene and toluene concentration bins during the three types of episodic events. The markers represent mean values and whiskers represent 25th and 75th percentiles.

Since NO_x played an important role in controlling secondary products by influencing the fate of organic peroxy radicals (RO_2) (Kroll et al., 2006; Kroll et al., 2008; Nihill et al., 2021; Peng et al., 2019), correlations of NO_3^-/NACs ratios versus NO/NO_2 ratios were compared among different episodes (Figure S13). During the three local episodes, NO_3^-/NACs was all negatively correlated with NO/NO_2 ratios with R^2 ranging from 0.40 to 0.67. This suggested that the higher NO/NO_2 ratios under the influence of local air masses greatly hindered local OH level and RO_2 branching chemistry was dominant under this high NO environment. In contrast, no correlation was observed between NO_3^-/NACs and NO/NO_2 ratios during mixed-influence and transport episodes, which may be attributable to the dominant role of OH reactions in both nitrate and NACs formations.

Both DHOPA and NACs are secondarily derived from mono-aromatics, with DHOPA being a benzene-ring opening product while NACs being ring-retaining products. We examined the variation pattern of the DHOPA/NACs ratio under different RH and O_x level bins (Figure S14a). An evident gradient was noted as a function of RH and O_x when O_x concentration level was lower than 65 ppb. Under conditions of higher RH and lower Ox, higher DHOPA/NACs was revealed, suggesting more conducive conditions for aqueous-phase processing in forming more-oxidized SOA. No clear trend was observed for DHOPA/NACs ratios when O_x level was higher than 65 ppb. It is likely that when atmospheric oxidation capacity was enhanced, the competition between benzene-ring addition and open reactions were affected by multiple factors (e.g., abundance

of VOC precursors, air masses).

Similar conclusion can be deduced from the variations of NACs versus BBtracers ratios (Figure S14b). The ratios presented the highest values on the left-top corner and experienced small changes as RH increased when O_x was less than 55 ppb, indicating that gas-phase photooxidation is a more dominant pathway for the formation of NACs in winter Shanghai. Previous studies also showed that high atmospheric oxidation capacity facilitated the transformation of mono-aromatics into particle-phase NACs and increased NACs concentrations substantially (Salvador et al., 2021; Yuan et al., 2016).

3.3.3 Dicarboxylic acids and hydroxyl dicarboxylic acids (DCAs and hDCAs)

For all three types of haze episodes, L_DCAs and L_hDCAs were observed to increase significantly. Their good correlations with nitrate, sulfate, and MO-OOA reflected that they were mainly formed via secondary processes. To further provide implications for their precursor sources and aging processes, diagnostic ratios of DCAs and hDCAs during episodic and non-episodic periods are examined as a function of O_x and RH in Figure 6. On the one hand, both succinic acid (C_4) and glutaric acid (C_5) could be formed from a wild range of precursors of longer carbon chains, while C_4 could also be the product of C_5 via undergoing successive oxidation cleavage (Ervens et al., 2004; Kawamura and Bikkina, 2016; Yang et al., 2008). On the other hand, C_4 can be further oxidized by OH radical to form malic acid (hC_4) (Ervens et al., 2004; Yang et al., 2008). Therefore, the ratios of C_4/C_5 and hC_4/C_4 could be applied to indicate the oxidizing degree of organic aerosols and the extent of photooxidation in the atmosphere (Yu et al., 2021). An examination of episode-specific showed that the average values of C_4/C_5 ratios and hC_4/C_4 ratios generally increased with O_x level during both episodic events and non-episodic periods (Figures 6a and 6b). In addition, the hC_4/C_4 ratios also displayed significantly positive correlations with RH during both episodic and non-episodic periods (Figure 6e). A previous field study also observed elevated hC_4/C_4 ratios with the increase of RH during wet season, attributing to the aqueous-phase processing of dicarboxylic acids (Yu et al., 2021). The hC_4/C_4 ratios elevated more rapidly during non-episodic periods compared with episodic periods. This may suggest that aqueous phase OH oxidation played a more important role in SOA formation during non-episodic periods as higher levels of O_3 were observed during non-episodic periods in reference to episodic events under the same RH level bins. In addition, the higher influence from marine air masses during non-episodic periods may also facilitate the formation of hC_4 as previous studies also observed high mole fraction of hydroxyl groups in marine aerosols (Aluwihare et al., 1997; Lyu et al., 2020; Russell et al., 2011). On the contrary, the C_4/C_5 ratios did not show clear trend with the increase of RH (Figure 6d), indicating that their dominant chemistry was insensitive to aqueous-phase processing, consistent with our understanding that the gas-phase photochemical oxidation played a more important role in the formation of DCAs.

In urban atmospheres, long-chain fatty acids, especially C_{16} and C_{18} fatty acids, are dominantly sources from primary cooking emissions. Azelaic acid (C_9 DCA) is a major photooxidation product of unsaturated C_{18} fatty acids (He et al., 2004; Kawamura et al. 1996; Robinson et al. 2006; Rogge et al. 1991). Hence, C_9 DCA/sFAs ratio reflects the oxidation degree of cooking organic aerosols. As shown in Figure 6f, C_9 FCA/sFAs ratios significantly increased with O_x, while RH had a minor influence on the oxidation of fatty acids. Such speculation was also supported by previous field observation and chamber experiments that O_3 acted as a predominant oxidant on the degradation of fatty acids (Vesna et al., 2009; Wang and Yu, 2021; Zahardis et al., 2007; Ziemann et al., 2005).
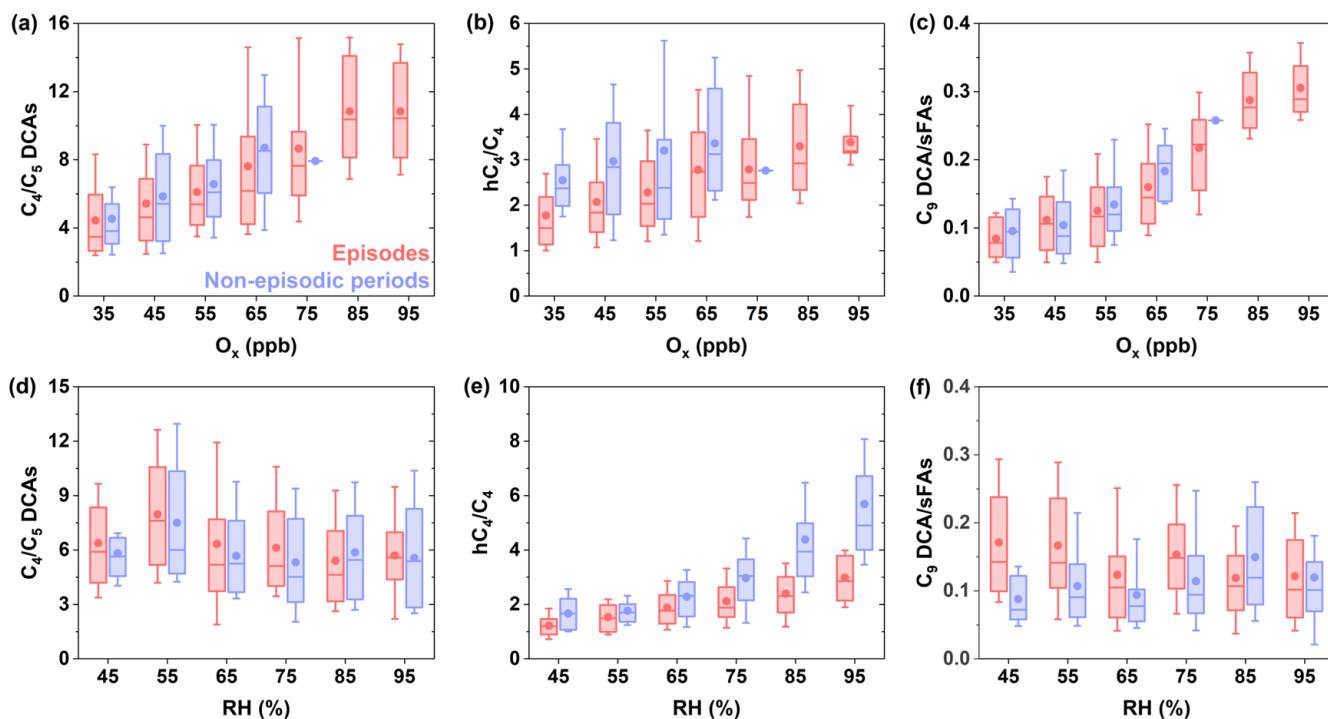
Figure 6. Ratios of (a) C_4/C_5, (b) hC_4/C_4, (c) $C_9/sFAs$ as a function of O_x concentration bins, and (d) C_4/C_5, (e) hC_4/C_4, (f) $C_9/sFAs$ as a function of RH level bins during episodic and non-episodic events.

4. Conclusions

The implementation of the Air Pollution Prevention and Control Action Plan since 2013 has profoundly altered $PM_{2.5}$ chemical composition in China, with one consequence being organic aerosol constituting an increasing fraction in recent years. Yet, comprehensive understanding of the physical and chemical processing of OA has been limited. This study presents bi-hourly measurements of 98 organic molecular markers and compares their mass contributions to $PM_{2.5}$ during different types of episodes at an urban site in Shanghai, a megacity in China. The average mass concentrations of total TAG-measured OA ranged from 934 to 1595 ng/m^3 during the nine observed haze episodes, which were 2-3 times higher than that during non-episodic periods (476 ng/m^3). Enhanced OA formation was a major culprit to the deterioration of $PM_{2.5}$ pollution in wintertime in Shanghai. Major contributors of OA were substantially different among local, mixed-influence and transport episodes. Local episodes were characterized by higher contributions from primary OA markers indicative of vehicular exhaust and cooking emissions, such as alkanes, hopanes, and fatty acids, accounting for 43% of the total TAG-measured OA mass in average. The SOA markers (e.g., DHOPA, C_9 acids) derived from these source categories also exhibited higher concentrations during local episodes. Specifically, the estimated mass contributions of aromatic SOA elevated from 21% during non-episodic periods to 44% during local episodes, indicating the important impacts from vehicular emissions on local aerosol formation.

In comparison, BBtracers comprised a significant contributor of primary OA during mixed-influence and transport episodes. The significant presence of BBtracers in urban $PM_{2.5}$ in Shanghai implicated the continued practice of burning agricultural residuals despite recent policies of banning such activities. Consistently, Ar-PCAs and NACs, which are indicative of secondary biomass burning sources, constituted larger fractions of the total TAG-measured OA during mixed-influence and transport episodes compared with local episodes. The positive correlations between NACs/BBtracers ratios and O_x during the campaign revealed that transformation of aromatics (e.g., benzene, toluene) from biomass burning via photochemical

processing wads an important source of NACs in wintertime in Shanghai. Besides, highly oxidized secondary organic molecular groups, L_DCAs and L_hDCAs, were also more abundant during mixed-influence and transport episodes under the aging of continental outflows, with contributions ranging from 39% to 57% in the total TAG-measured OA. During local episodes, L_DCAs and L_hDCAs were comparatively deficient while SemiASOA in TotalASOA were relatively higher. Such results were likely attributable to a suppression of atmospheric oxidative capacity under high NO_x concentrations. The fact that L_DCAs and L_hDCAs tracked well with O_x also supported their photochemical origin.

Overall, the significant variations in OA composition during different types of episodes indicate that the sources and formation processes of OA were diverse, subjecting to the influence of the prevailing air masses. Control of local urban sources such as vehicular and cooking emissions would lessen severity of local episodes while regional control of precursors for secondary inorganic aerosols and more effective restriction of biomass burning activities would reduce $PM_{2.5}$ episodes under synoptic conditions conducive for regional transport.

Data availability. The bi-hourly organic markers and other hourly chemical speciation data presented in this study are available from the data repository maintained by HKUST: https://doi.org/10.14711/dataset/ PXEV3I.

Author contributions. SZ, CH and JZY conceived the study and led the overall research. SZ made the overall data analysis with contributions from QW and SW. MZ and LQ collected and processed chemical species data measured by MARGA, OCEC analyzer and XRF. DDH collected and processed AMS measurement data. YG, SJ, QW and HW collected and processed VOCs measurement data. CC conducted background research and reviewed the writing. SZ and JZY wrote the paper with contributions from all coauthors.

Competing interests. The contact author has declared that none of the authors has any competing interests.

Financial support. This research was supported by Shanghai 2021 "Science and Technology Innovation Action Plan" social development science and technology project (21DZ1202300). We also acknowledge funding support by the Research Grants Council of Hong Kong (R6011-18) and National Natural Science Foundation of China (41875161).

References

Al-Naiema, I., Offenberg, J. H., Madler, C. J., Lewandowski, M., Kettler, J., Fang, T. and Stone, E. A.: Secondary organic aerosols from aromatic hydrocarbons and their contribution to fine particulate matter in Atlanta, Georgia, Atmospheric environment (1994), 223, 117227, 10.1016/j.atmosenv.2019.117227, 2020.

Aluwihare, L. I., Repeta, D. J. and Chen, R. F.: A major biopolymeric component to dissolved organic carbon in surface sea water, Nature (London), 387, 166-169, 10.1038/387166a0, 1997.

Cai, W., Li, K., Liao, H., Wang, H. and Wu, L.: Weather conditions conducive to Beijing severe haze more frequent under climate change, Nature climate change, 7, 257-262, 10.1038/nclimate3249, 2017.

Castro, L. M., Pio, C. A., Harrison, R. M. and Smith, D. J. T.: Carbonaceous aerosol in urban and rural European atmospheres: estimation of secondary organic carbon concentrations, Atmospheric environment (1994), 33, 2771-2781, 10.1016/S1352-2310(98)00331-8, 1999.

Chen, H. and Wang, H.: Haze Days in North China and the associated atmospheric circulations based on daily visibility data from 1960 to 2012, Journal of geophysical research.Atmospheres, 120, 5895-5909, 10.1002/2015JD023225, 2015.

Chen, L., Shi, M., Gao, S., Li, S., Mao, J., Zhang, H., Sun, Y., Bai, Z. and Wang, Z.: Assessment of population exposure to $PM_{2.5}$ for mortality in China and its public health benefit based on BenMAP, Environmental pollution (1987), 221, 311-317, 10.1016/j.envpol.2016.11.080, 2017.

Ding, A., Huang, X., Nie, W., Chi, X., Xu, Z., Zheng, L., Xu, Z., Xie, Y., Qi, X., Shen, Y., Sun, P., Wang, J., Wang, L., Sun, J., Xiu-Qun Yang, Qin, W., Zhang, X., Cheng, W., Liu, W., Pan, L. and Fu, C.: Significant reduction of $PM_{2.5}$ in eastern China due to regional-scale emission control: evidence from SORPES in 2011–2018, Atmospheric chemistry and physics, 19, 11791-11801, 10.5194/acp-19-11791-2019, 2019.

Ervens, B., Feingold, G., Frost, G. J. and Kreidenweis, S. M.: A modeling study of aqueous production of dicarboxylic acids: 1. Chemical pathways and speciated organic mass production, Journal of Geophysical Research: Atmospheres, 109, D15205-n/a, 10.1029/2003JD004387, 2004.

Fan, S., Gao, C. Y., Wang, L., Yang, Y., Liu, Z., Hu, B., Wang, Y., Wang, J. and Gao, Z.: Elucidating roles of near-surface vertical layer structure in different stages of $PM_{2.5}$ pollution episodes over urban Beijing during 2004–2016, Atmospheric environment (1994), 246, 118157, 10.1016/j.atmosenv.2020.118157, 2021.

Gao, Y., Wang, H., Zhang, X., Jing, S., Peng, Y., Qiao, L., Zhou, M., Huang, D. D., Wang, Q., Li, X., Li, L., Feng, J., Ma, Y. and Li, Y.: Estimating Secondary Organic Aerosol Production from Toluene Photochemistry in a Megacity of China, Environ. Sci. Technol., 53, 8664-8671, 10.1021/acs.est.9b00651, 2019.

Guo, B., Wang, Y., Zhang, X., Che, H., Zhong, J., Chu, Y. and Cheng, L.: Temporal and spatial variations of haze and fog and the characteristics of $PM_{2.5}$ during heavy pollution episodes in China from 2013 to 2018, Atmospheric pollution research, 11, 1847-1856, 10.1016/j.apr.2020.07.019, 2020.

He, L., Hu, M., Huang, X., Yu, B., Zhang, Y. and Liu, D.: Measurement of emissions of fine particulate organic matter from Chinese cooking, Atmospheric environment (1994), 38, 6557-6564, 10.1016/j.atmosenv.2004.08.034, 2004.

He, X., Huang, X. H. H., Chow, K. S., Wang, Q., Zhang, T., Wu, D. and Yu, J. Z.: Abundance and Sources of Phthalic Acids, Benzene-Tricarboxylic Acids, and Phenolic Acids in $PM_{2.5}$ at Urban and Suburban Sites in Southern China, ACS earth and space chemistry, 2, 147-158, 10.1021/acsearthspacechem.7b00131, 2018.

He, X., Wang, Q., Huang, X. H. H., Huang, D. D., Zhou, M., Qiao, L., Zhu, S., Ma, Y., Wang, H., Li, L., Huang, C., Xu, W., Worsnop, D. R., Goldstein, A. H. and Yu, J. Z.: Hourly measurements of organic molecular markers in urban Shanghai, China: Observation of enhanced formation of secondary organic aerosol during particulate matter episodic periods, Atmospheric environment (1994), 240, 117807, 10.1016/j.atmosenv.2020.117807, 2020.

Hu, D., Bian, Q., Li, T. W. Y., Lau, A. K. H. and Yu, J. Z.: Contributions of isoprene, monoterpenes, β-caryophyllene, and toluene to secondary organic aerosols in Hong Kong during the summer of 2006, J GEOPHYS RES-ATMOS, 113, D22206-n/a, 10.1029/2008JD010437, 2008.

Hu, D. and Yu, J. Z.: Secondary organic aerosol tracers and malic acid in Hong Kong: Seasonal trends and origins, ENVIRON CHEM, 10, 381-394, 10.1071/EN13104, 2013.

Huang, D. D., Zhu, S., An, J., Wang, Q., Qiao, L., Zhou, M., He, X., Ma, Y., Sun, Y., Huang, C., Yu, J. Z. and Zhang, Q.: Comparative Assessment of Cooking Emission Contributions to Urban Organic Aerosol Using Online Molecular Tracers and Aerosol Mass Spectrometry Measurements, Environ. Sci. Technol., 55, 14526–14535, 10.1021/acs.est.1c03280.

Huang, R., Zhang, Y., Bozzetti, C., Ho, K., Cao, J., Han, Y., Daellenbach, K. R., Slowik, J. G., Platt, S. M., Canonaco, F., Zotter, P., Wolf, R., Pieber, S. M., Bruns, E. A., Crippa, M., Ciarelli, G., Piazzalunga, A., Schwikowski, M., Abbaszade, G., Schnelle-Kreis, J., Zimmermann, R., An, Z., Szidat, S., Baltensperger, U., El Haddad, I. and Prévôt, A.,S.H.: High secondary aerosol contribution to particulate pollution during haze events in China, Nature, 514, 218-222, 10.1038/nature13774, 2014.

Kawamura, K. and Bikkina, S.: A review of dicarboxylic acids and related compounds in atmospheric aerosols: Molecular distributions, sources and transformation, Atmos. Res., 170, 140-160, 10.1016/j.atmosres.2015.11.018, 2016.

Kawamura, K., Kasukabe, H. and Barrie, L. A.: Source and reaction pathways of dicarboxylic acids, ketoacids and dicarbonyls in arctic aerosols: One year of observations, Atmospheric environment (1994), 30, 1709-1722, 10.1016/1352-2310(95)00395-9, 1996.

Kreisberg, N. M., Hering, S. V., Williams, B. J., Worton, D. R. and Goldstein, A. H.: Quantification of Hourly Speciated Organic Compounds in Atmospheric Aerosols, Measured by an In-Situ Thermal Desorption Aerosol Gas Chromatograph (TAG), Aerosol science and technology, 43, 38-52, 10.1080/02786820802459583, 2009.

540   Kroll, J. H., Ng, N. L., Murphy, S. M., Flagan, R. C. and Seinfeld, J. H.: Secondary Organic Aerosol Formation from Isoprene Photooxidation, Environ. Sci. Technol., 40, 1869-1877, 10.1021/es0524301, 2006.

Kroll, J. H. and Seinfeld, J. H.: Chemistry of secondary organic aerosol: Formation and evolution of low-volatility organics in the atmosphere, Atmospheric environment (1994), 42, 3593-3624, 10.1016/j.atmosenv.2008.01.003, 2008.

Li, M., Wang, T., Xie, M., Li, S., Zhuang, B., Huang, X., Chen, P., Zhao, M. and Liu, J.: Formation and Evolution Mechanisms for Two Extreme Haze Episodes in the Yangtze River Delta Region of China During Winter 2016, Journal of geophysical

545   research. Atmospheres, 124, 3607-3623, 10.1029/2019JD030535, 2019.

Li, Q., Zhang, R. and Wang, Y.: Interannual variation of the wintertime fog–haze days across central and eastern China and its relation with East Asian winter monsoon, Int. J. Climatol., 36, 346-354, 10.1002/joc.4350, 2016.

Li, X., Wang, Y., Hu, M., Tan, T., Li, M., Wu, Z., Chen, S. and Tang, X.: Characterizing chemical composition and light absorption of nitroaromatic compounds in the winter of Beijing, Atmospheric environment (1994), 237, 117712,

550   10.1016/j.atmosenv.2020.117712, 2020.

Lim, H. and Turpin, B. J.: Origins of Primary and Secondary Organic Aerosol in Atlanta: Results of Time-Resolved Measurements during the Atlanta Supersite Experiment, Environ. Sci. Technol., 36, 4489-4496, 10.1021/es0206487, 2002.

Liu, J., Li, J., Zhang, Y., Liu, D., Ding, P., Shen, C., Shen, K., He, Q., Ding, X., Wang, X., Chen, D., Szidat, S. and Zhang, G.: Source Apportionment Using Radiocarbon and Organic Tracers for $PM_{2.5}$ Carbonaceous Aerosols in Guangzhou, South China:

555   Contrasting Local- and Regional-Scale Haze Events, Environ. Sci. Technol., 48, 12002-12011, 10.1021/es503102w, 2014.

Liu, M., Huang, Y., Ma, Z., Jin, Z., Liu, X., Wang, H., Liu, Y., Wang, J., Jantunen, M., Bi, J. and Kinney, P. L.: Spatial and temporal trends in the mortality burden of air pollution in China: 2004–2012, Environ. Int., 98, 75-81, 10.1016/j.envint.2016.10.003, 2017.

Liu, Y., Wang, H., Jing, S., Peng, Y., Gao, Y., Yan, R., Wang, Q., Lou, S., Cheng, T. and Huang, C.: Strong regional transport

560   of volatile organic compounds (VOCs) during wintertime in Shanghai megacity of China, Atmospheric environment (1994), 244, 117940, 10.1016/j.atmosenv.2020.117940, 2021.

Lyu, X., Guo, H., Yao, D., Lu, H., Huo, Y., Xu, W., Kreisberg, N., Goldstein, A. H., Jayne, J., Worsnop, D., Tan, Y., Lee, S. and Wang, T.: In Situ Measurements of Molecular Markers Facilitate Understanding of Dynamic Sources of Atmospheric Organic Aerosols, Environ. Sci. Technol., 54, 11058-11069, 10.1021/acs.est.0c02277, 2020.

565   Ma, P., Zhang, P., Shu, J., Yang, B. and Zhang, H.: Characterization of secondary organic aerosol from photo-oxidation of gasoline exhaust and specific sources of major components, Environ. Pollut., 232, 65-72, 10.1016/j.envpol.2017.09.018, 2018.

Mao, L., Liu, R., Liao, W., Wang, X., Shao, M., Liu, S. C. and Zhang, Y.: An observation-based perspective of winter haze days in four major polluted regions of China, National science review, 6, 515-523, 10.1093/nsr/nwy118, 2019.

Nihill, K. J., Ye, Q., Majluf, F., Krechmer, J. E., Canagaratna, M. R. and Kroll, J. H.: Influence of the NO/NO_2 Ratio on

570   Oxidation Product Distributions under High-NO Conditions, Environ. Sci. Technol., 55, 6594-6601, 10.1021/acs.est.0c07621, 2021.

Peng, Z., Lee-Taylor, J., Orlando, J. J., Tyndall, G. S. and Jimenez, J. L.: Organic peroxy radical chemistry in oxidation flow reactors and environmental chambers and their atmospheric relevance, Atmospheric chemistry and physics, 19, 813-834, 10.5194/acp-19-813-2019, 2019.

575   Petit, J., Favez, O., Albinet, A. and Canonaco, F.: A user-friendly tool for comprehensive evaluation of the geographical origins of atmospheric pollution: Wind and trajectory analyses, Environmental modelling & software: with environment data news, 88, 183-187, 10.1016/j.envsoft.2016.11.022, 2017.

RenHe, Z., Li, Q. and Zhang, R.: Meteorological conditions for the persistent severe fog and haze event over eastern China in January 2013, Sci. China Earth Sci, 57, 26-35, 10.1007/s11430-013-4774-3, 2014.

580   Report on the State of the Ecology and Environment in China, 2019. Ministry of Ecology and Environment, the People's

Republic of China.

Robinson, A. L., Subramanian, R., Donahue, N. M., Bernardo-Bricker, A. and Rogge, W. F.: Source Apportionment of Molecular Markers and Organic Aerosol. 3. Food Cooking Emissions, Environ. Sci. Technol., 40, 7820-7827, 10.1021/es060781p, 2006.

585 Rogge, W. F., Hildemann, L. M., Mazurek, M. A., Cass, G. R. and Simoneit, B. R. T.: Sources of fine organic aerosol. 1. Charbroilers and meat cooking operations, Environ. Sci. Technol., 25, 1112-1125, 10.1021/es00018a015, 1991.

Russell, L. M., Bahadur, R. and Ziemann, P. J.: Identifying organic aerosol sources by comparing functional group composition in chamber and atmospheric particles, Proc. Natl. Acad. Sci. U. S. A., 108, 3516-3521, 10.1073/pnas.1006461108, 2011.

Salvador, C. M. G., Tang, R., Priestley, M., Li, L., Tsiligiannis, E., Le Breton, M., Zhu, W., Zeng, L., Wang, H., Yu, Y., Hu, M.,
590 Guo, S. and Hallquist, M.: Ambient nitro-aromatic compounds – biomass burning versus secondary formation in rural China, Atmospheric chemistry and physics, 21, 1389-1406, 10.5194/acp-21-1389-2021, 2021.

Schauer, J. J., Kleeman, M. J., Cass, G. R. and Simoneit, B.: Measurement of emissions from air pollution sources. 5. C-1-C-32 organic compounds from gasoline-powered motor vehicles, Environ. Sci. Technol., 36, 1169-1180, 10.1021/es0108077, 2002.

595 Sun, J., Gong, J., Zhou, J., Liu, J. and Liang, J.: Analysis of PM2.5 pollution episodes in Beijing from 2014 to 2017: Classification, interannual variations and associations with meteorological features, Atmospheric environment (1994), 213, 384-394, 10.1016/j.atmosenv.2019.06.015, 2019.

Tao, J., Zhang, L., Cao, J. and Zhang, R.: A review of current knowledge concerning $PM_{2.5}$ chemical composition, aerosol optical properties and their relationships across China, Atmospheric chemistry and physics, 17, 9485-9518, 10.5194/acp-17-
600 9485-2017, 2017.

Turpin, B. J. and Huntzicker, J. J.: Identification of secondary organic aerosol episodes and quantitation of primary and secondary organic aerosol concentrations during SCAQS, Atmospheric environment (1994), 29, 3527-3544, 10.1016/1352-2310(94)00276-Q, 1995.

Vesna, O., Sax, M., Kalberer, M., Gaschen, A. and Ammann, M.: Product study of oleic acid ozonolysis as function of humidity,
605 Atmospheric environment (1994), 43, 3662-3669, 10.1016/j.atmosenv.2009.04.047, 2009.

Wang, D., Zhou, B., Fu, Q., Zhao, Q., Zhang, Q., Chen, J., Yang, X., Duan, Y. and Li, J.: Intense secondary aerosol formation due to strong atmospheric photochemical reactions in summer: observations at a rural site in eastern Yangtze River Delta of China, Sci. Total Environ., 571, 1454-1466, 10.1016/j.scitotenv.2016.06.212, 2016.

Wang, H. L., Chen, C. H., Wang, Q., Huang, C., Su, L. Y., Huang, H. Y., Lou, S. R., Zhou, M., Li, L., Qiao, L. P. and Wang, Y.
610 H.: Chemical loss of volatile organic compounds and its impact on the source analysis through a two-year continuous measurement, Atmospheric environment, 80, 488-498, 10.1016/j.atmosenv.2013.08.040, 2013.

Wang, Q., He, X., Zhou, M., Huang, D. D., Qiao, L., Zhu, S., Ma, Y., Wang, H., Li, L., Huang, C., Huang, X. H. H., Xu, W., Worsnop, D., Goldstein, A. H., Guo, H. and Yu, J. Z.: Hourly Measurements of Organic Molecular Markers in Urban Shanghai, China: Primary Organic Aerosol Source Identification and Observation of Cooking Aerosol Aging, ACS earth and space
615 chemistry, 4, 1670-1685, 10.1021/acsearthspacechem.0c00205, 2020.

Wang, Q. and Yu, J. Z.: Ambient Measurements of Heterogeneous Ozone Oxidation Rates of Oleic, Elaidic, and Linoleic Acid Using a Relative Rate Constant Approach in an Urban Environment, Geophys. Res. Lett., 48, n/a, 10.1029/2021GL095130, 2021.

Wang, Q., Zhuang, G., Huang, K., Liu, T., Deng, C., Xu, J., Lin, Y., Guo, Z., Chen, Y., Fu, Q., Fu, J. S. and Chen, J.: Probing
620 the severe haze pollution in three typical regions of China: Characteristics, sources and regional impacts, Atmospheric environment (1994), 120, 76-88, 10.1016/j.atmosenv.2015.08.076, 2015.

Wang, Y. J., Hu, M., Wang, Y. C., Zheng, J., Shang, D. J., Yang, Y. D., Liu, Y., Li, X., Tang, R. Z., Zhu, W. F., Du, Z. F., Wu, Y. S., Guo, S., Wu, Z. J., Lou, S. R., Hallquist, M. and Yu, J. Z.: The formation of nitro-aromatic compounds under high NO_x and anthropogenic VOC conditions in urban Beijing, China, Atmospheric chemistry and physics, 19, 7649-7665, 10.5194/acp-
625 19-7649-2019, 2019.

Wang, Y., Li, L., Chen, C., Huang, C., Huang, H., Feng, J., Wang, S., Wang, H., Zhang, G., Zhou, M., Cheng, P., Wu, M., Sheng, G., Fu, J., Hu, Y., Russell, A. G. and Wumaer, A.: Source apportionment of fine particulate matter during autumn haze episodes in Shanghai, China, Journal of geophysical research. Atmospheres, 119, 1903-1914, 10.1002/2013JD019630, 2014a.

Wang, Y., Yao, L., Wang, L., Liu, Z., Ji, D., Tang, G., Zhang, J., Sun, Y., Hu, B. and Xin, J.: Mechanism for the formation of the January 2013 heavy haze pollution episode over central and eastern China, Sci. China Earth Sci, 57, 14-25, 10.1007/s11430-013-4773-4, 2014b.

Wei, X., Liu, M., Yang, J., Du, W., Sun, X., Huang, Y., Zhang, X., Khalil, S. K., Luo, D. and Zhou, Y.: Characterization of $PM_{2.5}$-bound PAHs and carbonaceous aerosols during three-month severe haze episode in Shanghai, China: Chemical composition, source apportionment and long-range transportation, Atmospheric environment (1994), 203, 1-9, 10.1016/j.atmosenv.2019.01.046, 2019.

Williams, B. J., Goldstein, A. H., Kreisberg, N. M. and Hering, S. V.: An In-Situ Instrument for Speciated Organic Composition of Atmospheric Aerosols: Thermal Desorption Aerosol GC/MS-FID (TAG), Aerosol science and technology, 40, 627-638, 10.1080/02786820600754631, 2006.

Yan, C., Zheng, M., Bosch, C., Andersson, A., Desyaterik, Y., Sullivan, A. P., Collett, J. L., Zhao, B., Wang, S., He, K. and Gustafsson, Ö: Important fossil source contribution to brown carbon in Beijing during winter, Scientific reports, 7, 43182, 10.1038/srep43182, 2017.

Yang, L., Ray, M. B. and Yu, L. E.: Photooxidation of dicarboxylic acids—Part II: Kinetics, intermediates and field observations, Atmospheric environment (1994), 42, 868-880, 10.1016/j.atmosenv.2007.10.030, 2008.

Yao, L., Huo, J., Wang, D., Fu, Q., Sun, W., Li, Q. and Chen, J.: Online measurement of carbonaceous aerosols in suburban Shanghai during winter over a three-year period: Temporal variations, meteorological effects, and sources, Atmospheric environment (1994), 226, 117408, 10.1016/j.atmosenv.2020.117408, 2020.

Yu, Q., Chen, J., Cheng, S., Qin, W., Zhang, Y., Sun, Y. and Ahmad, M.: Seasonal variation of dicarboxylic acids in $PM_{2.5}$ in Beijing: Implications for the formation and aging processes of secondary organic aerosols, Sci. Total Environ., 763, 142964, 10.1016/j.scitotenv.2020.142964, 2021.

Yuan, B., Liggio, J., Wentzell, J., Li, S., Stark, H., Roberts, J. M., Gilman, J., Lerner, B., Warneke, C., Li, R., Leithead, A., Osthoff, H. D., Wild, R., Brown, S. S. and de Gouw, J.,A.: Secondary formation of nitrated phenols: insights from observations during the Uintah Basin Winter Ozone Study (UBWOS) 2014, Atmospheric chemistry and physics, 16, 2139-2153, 10.5194/acp-16-2139-2016, 2016.

Zahardis, J. and Petrucci, G. A.: The oleic acid-ozone heterogeneous reaction system: products, kinetics, secondary chemistry, and atmospheric implications of a model system – a review, Atmospheric chemistry and physics, 7, 1237-1274, 10.5194/acp-7-1237-2007, 2007.

Zeng, L., Huang, D. D., Zhu, S., Li, F., Zhou, M., Qiao, L., Wang, Q., Wang, Q., Ma, Y., Lou, S., Shi, H., In Hoi, K., Mok, K. M., Ge, X., Wang, H., Yu, J. Z., Huang, C. and Li, Y. J.: The interplays among meteorology, source, and chemistry in high particulate matter pollution episodes in urban Shanghai, China, Sci. Total Environ., 853, 158347, 10.1016/j.scitotenv.2022.158347, 2022.

Zhang, J., He, X., Gao, Y., Zhu, S., Jing, S., Wang, H., Yu, J. Z. and Ying, Q.: Assessing Regional Model Predictions of Wintertime SOA from Aromatic Compounds and Monoterpenes with Precursor-specific Tracers, Aerosol and air quality research, 21, 210233, 10.4209/aaqr.210233, 2021a.

Zhang, J., He, X., Gao, Y., Zhu, S., Jing, S., Wang, H., Yu, J. Z. and Ying, Q.: Estimation of Aromatic Secondary Organic Aerosol Using a Molecular Tracer – A Chemical Transport Model Assessment, Environ. Sci. Technol., 55, 12882-12892, 10.1021/acs.est.1c03670, 2021b.

Zhang, X. Y., Wang, Y. Q., Niu, T., Zhang, X. C., Gong, S. L., Zhang, Y. M. and Sun, J. Y.: Atmospheric aerosol compositions in China: spatial/temporal variability, chemical signature, regional haze distribution and comparisons with global aerosols, Atmospheric chemistry and physics, 12, 779-799, 10.5194/acp-12-779-2012, 2012.

Zhao, M., Qiao, T., Huang, Z., Zhu, M., Xu, W., Xiu, G., Tao, J. and Lee, S.: Comparison of ionic and carbonaceous

compositions of PM$_{2.5}$ in 2009 and 2012 in Shanghai, China, Sci. Total Environ., 536, 695-703, 10.1016/j.scitotenv.2015.07.100, 2015.

Zhao, X. J., Zhao, P. S., Xu, J., Meng, W., Pu, W. W., Dong, F., He, D. and Shi, Q. F.: Analysis of a winter regional haze event and its formation mechanism in the North China Plain, Atmospheric chemistry and physics, 13, 5685-5696, 10.5194/acp-13-5685-2013, 2013.

Zhu, S., Wang, Q., Qiao, L., Zhou, M., Wang, S., Lou, S., Huang, D., Wang, Q., Jing, S., Wang, H., Chen, C., Huang, C. and Yu, J. Z.: Tracer-based characterization of source variations of PM$_{2.5}$ and organic carbon in Shanghai influenced by the COVID-19 lockdown, Faraday Discuss., 226, 112-137, 10.1039/D0FD00091D, 2021.

Zhu, W., Zhou, M., Cheng, Z., Yan, N., Huang, C., Qiao, L., Wang, H., Liu, Y., Lou, S. and Guo, S.: Seasonal variation of aerosol compositions in Shanghai, China: Insights from particle aerosol mass spectrometer observations, Sci. Total Environ., 771, 144948, 10.1016/j.scitotenv.2021.144948, 2021.

Ziemann, P. J.: Aerosol products, mechanisms, and kinetics of heterogeneous reactions of ozone with oleic acid in pure and mixed particles, Faraday Discuss., 130, 469, 10.1039/b417502f, 2005.